Point Defects and Diffusion in Paratellurite

J. Wegener [a], O. Kanert [a], R. Küchler [a], and A. Watterich [b]

[a] Institute of Physics, University of Dortmund, 44221 Dortmund, Germany
[b] Research Laboratory for Crystal Physics, Budapest, Hungary

Z. Naturforsch. **49a**, 1151–1158 (1994); received August 22, 1994

Dedicated to Professor Werner Müller-Warmuth on the occasion of his 65th birthday

^{125}Te nuclear spin relaxation (NSR) and electrical conductivity measurements were performed on ultrapure single-crystalline paratellurite (α-TeO_2) between about 50 K and the melting point (1007 K) at various oxygen partial pressures (1 bar – 10^{-4} bar). At elevated temperatures the NSR rate $1/T_1$ and conductivity σ are caused by the diffusive motion of point defects. From the observed p_{O_2}-dependence of $1/T_1$ and σ a defect model is developed which is shown to be consistent with the experimental data. The model involves ionic oxygen interstitials (O_i''), doubly charged oxygen vacancies ($V_O^{\bullet\bullet}$) and charge-compensating electron holes ($h^\bullet$). The observed pressure dependence suggests that the NSR rate is induced by the motion of $V_O^{\bullet\bullet}$ while the conductivity is due to the mobility of $h^\bullet$. Evaluation of the data leads to 3.3 eV for the incorporation enthalpy of oxygen on interstitial sites and to 4.5 eV for the formation enthalpy of oxygen Frenkel pairs ($O_i'' - V_O^{\bullet\bullet}$). Further, the chemical diffusion coefficient D^c is found to be caused by the ambipolar diffusion of O_i'' and $h^\bullet$. At 950 K we obtained from both the NSR and conductivity experiments $D^c = (1 \pm 0.3) \cdot 10^{-5}$ cm^2/s.

Key words: Oxides, Point defects, Diffusion, NMR, Conductivity.

1. Introduction

Paratellurite (α-TeO_2) is an insulator with a gap energy of about 4.3 eV [1], and crystallizes in the space group $P4_12_12$. Measurements of piezoelectric and photoelastic properties [2, 3] of the transparent material suggested its practical application as deflector, light modulator, and tunable optical filter. It shows an extremely slow velocity of shear wave propagation along the ⟨110⟩-directions, low acoustic losses and a high refractive index and corresponding dielectric constant [4].

As depicted in Fig. 1, the ^{125}Te NMR spectrum of α-TeO_2 consists of four well-separated lines according to four magnetically non-equivalent Te lattice sites in the tetragonal unit cell. The width of the individual lines was found to be about 400 Hz independent of the crystal orientation with respect to the magnetic field direction. The observed value is somewhat larger than the dipolar contribution obtained by Van Vleck's relation. Hence, we conclude that part of the width is caused by small misalignments of the Chemical Shift (CS) tensor due to lattice imperfections or demagnetisation effects. In this context one should note that ^{125}Te has a nuclear spin $I = 1/2$, i.e. one does not expect any quadrupole effects. From the rotation pattern of the lines, the size and orientation of the CS-tensor relative to the crystal axes have been determined (see inset of Figure 1). We obtained at room temperature [5]

$$\tilde{\sigma} = 317 \text{ ppm} + \begin{pmatrix} -734 & & \\ & 122 & \\ & & 612 \end{pmatrix} \text{ppm},$$

using a value of 13.451 MHz/T as reference. The first principal axis is along the ⟨110⟩-direction resulting directly from the symmetry of the Te sites. The angle

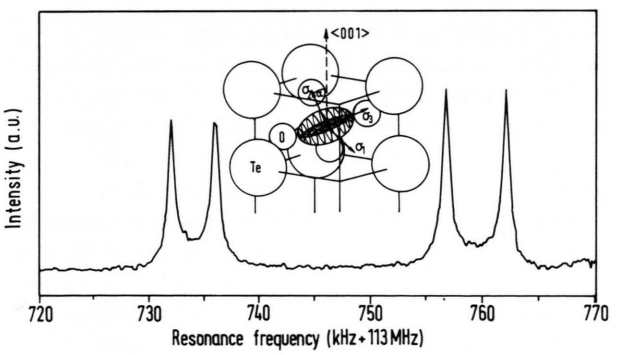

Fig. 1. ^{125}Te spectrum in single crystalline α-TeO_2 observed at room temperature. Inset: Position of the CS-tensor ellipsoid at a Te site as obtained from the rotation pattern of the NMR spectrum.

Reprint requests to Dr. O. Kanert.

0932-0784 / 94 / 1200-1151 $ 06.00 © – Verlag der Zeitschrift für Naturforschung, D-72027 Tübingen

α between the second principal axis and the $\langle 001 \rangle$-direction is found to be 20.5°, which agrees roughly to the angle of 17° between the $\langle 001 \rangle$-direction and the normal of the O–Te–O plane, i.e. the third principal axis lies approximately in the O–Te–O plane.

The spectrum was found to be shifted linearly to higher frequencies with rising temperature [5]. The observed temperature dependence of the shift can be explained on the basis of a Debye model for the phonon-induced contribution to the local field, $B(T)$, due to the CS-interaction: The model yields $B(T) \propto T$ for $T > \Theta_{\text{Debye}}$ and $B(T) \propto T^4$ for $T < \Theta_{\text{Debye}}$ independent of the actual density of phonon states ($\Theta_{\text{Debye}} = 265$ K) [6]).

To our knowledge only two investigations have been carried out in the past on the diffusion properties of α-TeO_2 [7, 8]. Both studies deal with the temperature dependence of the electrical conductivity at elevated temperatures. The authors observed a curvature in the Arrhenius representation of the data and concluded that two different mechanisms are responsible for the conductivity. Below about 800 K the conductivity is ionic, probably due to extrinsic oxygen-ion vacancies whereas above 800 K the conductivity is caused by intrinsic electronic carriers. In the present paper we develop a defect model which is able to explain consistently both the temperature dependence and the oxygen partial pressure (p_{O_2}) dependence of the motion-induced ^{125}Te NSR rate and electrical conductivity observed in pure single-crystalline α-TeO_2.

2. Experimental

Optically clear paratellurite single crystals of high quality were obtained from the Research Laboratory for Crystal Physics in Budapest/Hungary. The amount of impurities was smaller than 5 ppm. The size of the NMR-samples was typically $10 \times 10 \times 15$ mm; the samples for electrical conductivity measurements were prepared by cutting 2 mm thin disks with a diameter of 8 mm. Symmetry axis of the disks was along $\langle 110 \rangle$-direction. After polishing the surface, plane Pt-electrodes were pressed on both sides of the sample by means of a force-controlled piston device [9].

The NMR experiments were performed under two different field strengths (6.3 T and 8.5 T, respectively) using an upgraded Bruker SXP 4-100 pulse NMR spectrometer including an on-line data acquisition system. The ^{125}Te spectra were obtained from Fourier transformation of the off-resonance free induction decay following a short $\pi/2$-pulse, while the NSR rates $1/T_1$ were measured by a saturation sequence (pulse series-τ-$\pi/2$). The NMR experiments below room temperature were performed with a commercial gas-flow He-cryostat (Leybold) which could be temperature-controlled within an accuracy of about 0.5 K. Most of the NMR experiments were carried out between room temperature and 1000 K under different oxygen partial pressures. Details of the corresponding high-temperature probe assembly and of the oxygen partial pressure device used for the NMR as well as for the conductivity experiments are published in [10]. The conductivity measurements were performed by means of a Schlumberger SI-1260 impedance meter and an electrometer-type preamplifier (Chelsea Dielectric) operating between 10 μHz and 10 MHz. Automatic control of the impedance meter and on-line data acquisition were realized by a PC. In order to investigate the diffusional properties of oxygen-induced defects in α-TeO_2 we have carried out two types of experiments:

i) Temperature dependence of the ^{125}Te NSR rate $1/T_1$ and conductivity σ under constant p_{O_2}-pressure.

ii) Time response of $1/T_1$ and σ after a sudden change of p_{O_2} at constant temperatures.

3. Nuclear Spin Relaxation

An Arrhenius plot of the temperature dependence of $1/T_1$ observed at two different p_{O_2}-pressures under two different magnetic field strengths is shown in Figure 2. The data can be interpreted in terms of two contributions, a phonon-induced contribution, $1/T_1|_{\text{Ph}}$, and a diffusion-induced contribution, $1/T_1|_{\text{Diff}}$, which becomes dominant above 800 K:

$$1/T_1 = 1/T_1|_{\text{Ph}} + 1/T_1|_{\text{Diff}} \,. \tag{1}$$

As depicted in Fig. 3 in a log-log presentation, the temperature dependence of $1/T_1|_{\text{Ph}}$ follows a power law of the form $1/T_1|_{\text{Ph}} \propto T^n$ with $n = 2$ for $T \geq 300$ K and $n = 3$ for $50\text{ K} < T < 300$ K. This can be explained by a two-phonon (Raman) process using the following non-Debye DOS (Density of states) $g(\omega)$ for the phonons:

$$g(\omega) = g \begin{cases} \omega^2 \ldots \omega < \omega_{\text{D}} & (\triangleq 33\text{ K}), \\ \omega_{\text{D}}^2 \ldots \omega_{\text{D}} < \omega < \omega_{\max}, \\ 0 \quad \ldots \omega > \omega_{\max} & (\triangleq 1100\text{ K}). \end{cases} \tag{2}$$

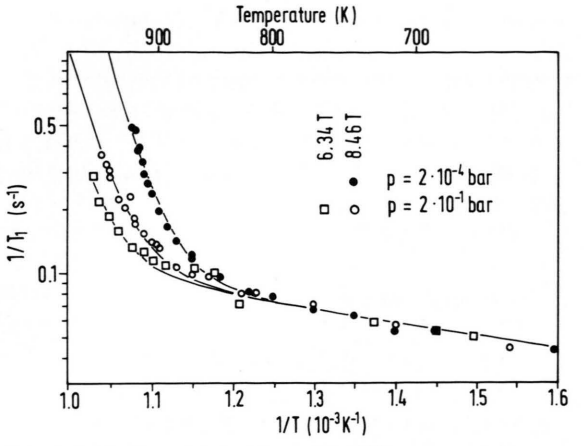

Fig. 2. Arrhenius presentation of the ^{125}Te NSR rate $1/T_1$ for two different p_{O_2}-pressures under two different magnetic field strengths. Solid lines are fits to the data by means of (7, 8).

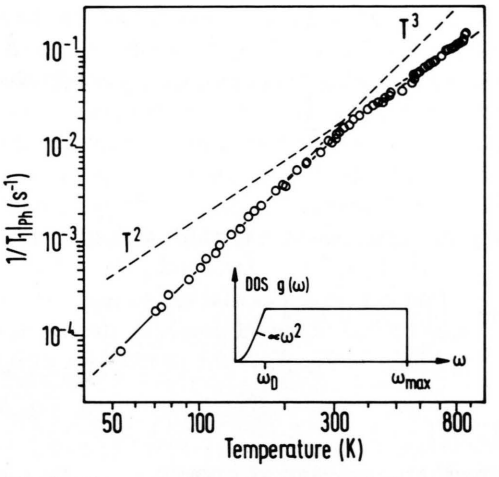

Fig. 3. Phonon-induced NSR rate $1/T_1|_{Ph}$ vs temperature. Solid line is a fit to the data by means of (4) using a DOS for the phonons as sketched in the figure.

The distribution in (2) is suggested by the large number of optical phonon modes of roughly equal strengths in α-TeO_2 [11].

Generally, the two-phonon-induced relaxation rate can be written as [12]

$$\left.\frac{1}{T_1}\right|_{Ph} = 4\pi\gamma^2 \sum_{i,j} |\varepsilon_i\, \varepsilon_j'\, B_{ij}|^2\, \delta(\omega_i - \omega_j - \omega_0). \quad (3)$$

Here $\varepsilon_i = q_i(\hbar/2\varrho\,\omega_i)^{1/2}\sqrt{n_i}$ denotes strain due to the annihilation of a phonon with wave vector q_i, frequency ω_i and quantum number n_i, while $\varepsilon_j' = q_j(\hbar/2\varrho\,\omega_j)^{1/2}\sqrt{n_j+1}$ is the corresponding strain caused by the creation of a phonon of type j, ϱ is the density of the crystal, γ the gyromagnetic ratio of the probe nucleus, and $B_{ij} = \partial^2 B_\perp/\partial\varepsilon_i\,\partial\varepsilon_j \equiv b_2$ the strain induced variation of the component $B_\perp$ of the local field $\boldsymbol{B}$ (which couples to the nuclear spin) perpendicular to the external field $\boldsymbol{B}_0$. Introducing mean occupation numbers $\langle n\rangle = 1/(e^{-\hbar\omega/kT}-1)$ for n_i, n_j and taking into account that $q = \omega/v$ (v: sound velocity) and $\omega_i, \omega_j \gg$ Larmor frequency ω_0, (3) can be rewritten by replacing the summation over i, j by an integration over the DOS $g(\omega)$ as

$$\left.\frac{1}{T_1}\right|_{Ph} = \text{const} \int_0^{\omega_{max}} d\omega\, b_2^2\, \omega^2\, g^2(\omega)\, \frac{e^{\hbar\omega/kT}}{(e^{\hbar\omega/kT}-1)^2}. \quad (4)$$

At low temperatures ($kT \ll \hbar\,\omega_{max}$) one obtains a power law

$$\left.\frac{1}{T_1}\right|_{Ph} \propto T^{2n+3} \quad (5a)$$

for the phonon-induced NSR rate assuming $g(\omega) \propto \omega^n$. Hence, a Debye DOS ($n = 2$) leads to $1/T_1|_{Ph} \propto T^7$ often observed in NMR and ESR experiments. A frequency independent DOS, however, as proposed by (2) for $T \gtrsim 33$ K, yields $1/T_1|_{Ph} \propto T^3$ in accord with the low temperature data shown in Figure 3.

At high temperatures ($kT \gg \hbar\,\omega_{max}$), expansion of the exponentials in (4) leads to the well known T^2-relation independent of $g(\omega)$

$$\left.\frac{1}{T_1}\right|_{Ph} \propto T^2 \int_0^{\omega_{max}} d\omega\, g^2(\omega) \propto T^2 \quad (5b)$$

in agreement with the NSR rates observed above about 300 K (see Figure 3). The solid line in Fig. 3 is a fit to the data by means of (4) using a DOS $g(\omega)$ as given by (2), and sketched in the inset of Figure 3.

We have measured the phonon-induced NSR rate $1/T_1|_{Ph}$ at different magnetic fields B_0 down to about 10^{-2} T by means of a field-cycling technique. Surprisingly, we did not find any field dependence of $1/T_1|_{Ph}$, i.e. the relaxation process is not caused by phonon-induced fluctuations of the CS-tensor; for which one expects $1/T_1|_{Ph} \propto B_0^2$. As ^{125}Te does not possess a nuclear quadrupole moment, one has to conclude that the underlying phonon-spin interaction is of magnetic origin, probably electron-coupled (pseudo) spin-spin interaction [13, 14] or a kind of spin-rotation interaction [15].

Further, the phonon-induced NSR rate was found to depend on the orientation of the crystal with re-

spect to the magnetic field direction. For a rotation around the ⟨001⟩-axis, where the four-line spectrum degenerates into a two-line spectrum, the phonon-induced relaxation rate of the two lines is given by

$$\left.\frac{1}{T_1}\right|_{\mathrm{Ph}} = a \pm b \sin(2\Theta), \tag{6a}$$

where Θ denotes the angle between the ⟨100⟩ axis and $\boldsymbol{B}_0$, and $a = 11.7 \cdot 10^{-3}\,\mathrm{s}^{-1}$ and $b = 4.47 \cdot 10^{-3}\,\mathrm{s}^{-1}$ at room temperature. The observed angular dependence reflects the asymmetry of the local field $\boldsymbol{B}$ responsible for the relaxation process: The strength of the NSR rate is given by the components $B_\perp$ of the local field perpendicular to $\boldsymbol{B}_0$, i.e.

$$1/T_1|_{\mathrm{Ph}} \propto \overline{B_\perp^2} = \overline{B^2 - B_z^2} = \mathrm{const} - \sum_{i,j} \overline{B_i B_j} n_i n_j \tag{6b}$$

with $n_i = \cos(\boldsymbol{B}_0, \text{crystal axis } i)$. Equation (6a) follows directly from (6b) for a rotation of the crystal as performed in the experiment.

In the entire temperature range the data shown in Fig. 2 were evaluated by means of the relation

$$\begin{aligned} 1/T_1 &= 1/T_1|_{\mathrm{Ph}} + 1/T_1|_{\mathrm{Diff}} \\ &= a(\Theta)\, T^2 + b(\omega_0, p_{\mathrm{O}_2}) \exp(-E_{\mathrm{NMR}}/kT). \end{aligned} \tag{7}$$

Contrary to the coefficient $a = a(\Theta)$, the coefficient b does not depend on the orientation of the crystal relative to the magnetic field direction, indicating an isotropic diffusion process. Analysis of the data leads to the relation

$$1/T_1|_{\mathrm{Diff}} \propto \omega_0^2\, p_{\mathrm{O}_2}^{-1/6} \exp(-3.0\,\mathrm{eV}/kT) \tag{8}$$

for the diffusion-induced NSR rate, which is consistent with the following mechanism: The NSR rate is induced by the diffusion of point defects of concentration $\{V\}$ and hopping rate $\Gamma_V = \Gamma_{V0} \exp(-H_\mathrm{m}/kT)$, where H_m is the corresponding migration enthalpy. The relaxation process occurs via fluctuations of the CS-tensor when a point defect encounters a ^{125}Te probe nucleus. Then, assuming $\Gamma_V > \omega_0$, the standard relations of diffusion-induced NSR [15] lead to

$$\begin{aligned} 1/T_1|_{\mathrm{Diff}} &\propto \omega_0^2 \{V(p_{\mathrm{O}_2}, T)\}/\Gamma_V \\ &\propto \omega_0^2 \{V(p_{\mathrm{O}_2})\} \exp\left(-\frac{H_V - H_m}{kT}\right) \end{aligned} \tag{9}$$

with H_V being the formation enthalpy of the point defects. The condition $\Gamma_v > \omega_0$ is supported by results of additional $T_{1\varrho}$-experiments: The temperature dependence of $1/T_{1\varrho}$ does not exhibit a maximum and was found to be equal to $1/T_1$ (Fig. 2), indicating that fluctuations on the time scale of ms do not exist. Comparison of (8) with (9) yields $\{V(p_{\mathrm{O}_2})\} \propto p_{\mathrm{O}_2}^{-1/6}$. The solid lines in Fig. 2 are fits to the data using as best-fit parameters $a = 1.14 \cdot 10^{-7}\,\mathrm{s}^{-1}\,\mathrm{K}^{-2}$, b (8.5 T, $2 \cdot 10^{-4}$ bar) $= 49 \cdot 10^{-14}\,\mathrm{s}^{-1}$ and b (6.4 T, 0.2 bar) $= 5 \cdot 10^{-14}\,\mathrm{s}^{-1}$.

4. Electrical Conductivity

The observed temperature and p_{O_2}-dependence of the conductivity σ is depicted in Figure 4. The data can be related to three thermally activated processes according to

$$\sigma T = T \sum_{i=1}^{3} \sigma_i = \sum_{i=1}^{3} a_i(p_{\mathrm{O}_2}) \exp(-E_i/kT) \tag{10}$$

with the following activation energies: $E_1 = 0.44 \pm 0.02$ eV, $E_2 = 1.1 \pm 0.1$ eV, $E_3 = 2.4 \pm 0.2$ eV. The first and third contribution are found to be independent of p_{O_2}, while the second contribution depends on p_{O_2}. We obtained $a_2 \propto p_{\mathrm{O}_2}^{-1/6}$. Following Hartmann [8], we assume that the first contribution is due to the migration of impurity-controlled (i.e. extrinsic) charged vacancies, i.e. $E_1 = H_\mathrm{m}$, whereas the magnitude of E_3 indicates an intrinsic semiconduction for the third contribution: $E_3 = 1/2\, E_{\mathrm{gap}}$. The defect model presented in the next section demonstrates that the second contribution can be related to the motion of electron holes $\mathrm{h}^\bullet$. The solid lines in Fig. 4 are fits to the data using

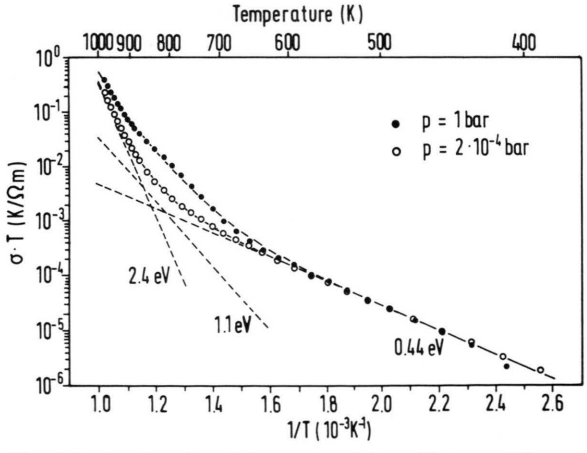

Fig. 4. Arrhenius plot of the conductivity σT at two different p_{O_2}-pressures. Solid lines are fits to the data by means of (10) consisting of three different processes as indicated in the diagram.

$a_1 = 3.5 \cdot 10^{-3}$ K/Ωm, $a_3 = 2 \cdot 10^{9}$ K/Ωm, a_2(0.2 bar) = 840 K/Ωm, and $a_2(2 \cdot 10^{-4}$ bar) = 120 K/Ωm as best-fit parameters.

5. Defect Model

A model of dilute, non-interacting point defects is developed for α-TeO_2. This model takes into account that, by ^{127}Te radio-tracer experiments, self-diffusion of Te was observed to be extremely slow up to the melting point ($D_{Te}(950\,K) \leq 10^{-15}$ cm^2/s), i.e. Te does not take part in internal defect-chemical reactions. Hence, only internal reactions of oxygen have to be considered.

In the following we use the Kröger-Vink notation [18] for the different relations. Oxygen gas (O_2(g)) is supposed to be incorporated as ionic oxygen O_i'' at vacant interstitial sites V_i under formation of electron holes $h^\bullet$:

$$\tfrac{1}{2}\,O_2(g) + V_i \leftrightarrow O_i'' + 2\,h^\bullet. \tag{11}$$

Considering that $p_{O_2} \propto \{O_2(g)\}$, the corresponding mass action law is given by

$$p_{O_2}^{-1/2}\,\{O_i''\}\,\{h^\bullet\}^2 \propto \exp\left(-\frac{H_S}{kT}\right), \tag{12}$$

where H_S denotes the solution enthalpy of oxygen. Further, Frenkel pairs consisting of O_i'' and doubly charged oxygen vacancies $V_O^{\bullet\bullet}$ are formed according to

$$O_O \leftrightarrow O_i'' + V_O^{\bullet\bullet}, \tag{13}$$

where O_O denotes a regular oxygen atom at an anion site. The mass action law of the Frenkel reaction is

$$\{O_i''\}\,\{V_O^{\bullet\bullet}\} \propto \exp\left(\frac{H_F}{kT}\right) \tag{14}$$

with H_F being the formation enthalpy of a Frenkel pair. Charge neutrality requires

$$2\,\{O_i''\} + \{e'\} = 2\,\{V_O^{\bullet\bullet}\} + \{h^\bullet\}. \tag{15}$$

The results of the time-response experiments in the next section reveal that oxygen vacancies are the minority charge carriers, i.e. $\{O_i''\} \gg \{V_O^{\bullet\bullet}\}$, and therefore $2\,\{O_i''\} = \{h^\bullet\}$ according to (15). Then, one obtains from (12) and (14)

$$\{h^\bullet\} \propto p_{O_2}^{+1/6} \exp\left(-\frac{\frac{1}{3}H_S}{kT}\right) \tag{16a}$$

and

$$\{V_O^{\bullet\bullet}\} \propto p_{O_2}^{-1/6} \exp\left(-\frac{H_F - \frac{1}{3}H_S}{kT}\right) \tag{16b}$$

for the concentration of electron holes and oxygen vacancies. The observed pressure dependence of the conductivity contribution σ_2 is in accord with (16a). Hence, we conclude that $\sigma_2\,T \propto \{h^\bullet\}$ and in consequence $H_S = 3\,E_2 = 3.3 \pm 0.3$ eV. Further, the measured pressure dependence of $1/T_1|_{Diff}$ agrees with (16b), indicating that the relaxation process is caused by the diffusion of the minority carriers $V_O^{\bullet\bullet}$, i.e. $\{V\} = \{V_O^{\bullet\bullet}\}$ in (9). Then, comparison of (8), (9), and (16b) yields $H_F = E_{NMR} + 1/3\,H_S + H_m = 4.5\,\text{eV} \pm 0.4\,\text{eV}$ for the formation enthalpy of oxygen Frenkel pairs (13), and $H_V = E_{NMR} + H_m = 3.4\,\text{eV} \pm 0.3\,\text{eV}$ for the formation enthalpy of oxygen vacancies using $H_m = E_1 = 0.44$ eV and $E_{NMR} = 3\,\text{eV} \pm 0.2$ eV.

6. Transient Experiments

As noted in Sect. 2, the time evolution of the conductivity and nuclear spin relaxation was measured after a sudden change of p_{O_2} at constant temperature. Results of such experiments are presented in Fig. 5 for the conductivity σ and in Fig. 6 for the ^{125}Te NSR rate $1/T_1$. The observed time response of σ and $1/T_1$ is opposite with respect to the sign of the p_{O_2}-change in accord with the observed pressure dependence of the two observables shown in Figs. 2 and 4. Further, the corresponding time constants of the response of $\sigma(t)$ are equal when raising (oxidation) or lowering (reduc-

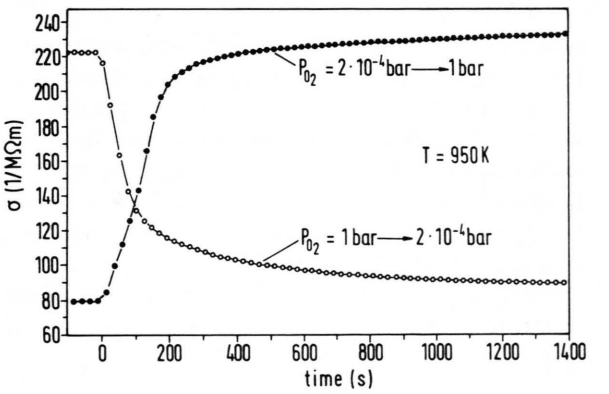

Fig. 5. Time response of the conductivity σ after a sudden change of p_{O_2} at 950 K. Solid lines are fits to the data by means of (18) using $D^c = (1 \pm 0.3) \cdot 10^{-5}$ cm^2/s.

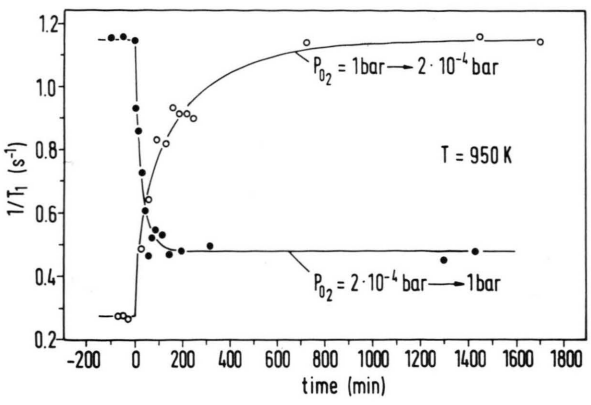

Fig. 6. Time response of $1/T_1$ of ^{125}Te after a sudden change of p_{O_2} at 950 K. Solid lines are fits to the data using $D^c = (1 \pm 0.3) \cdot 10^{-5}$ cm^2/s (see text).

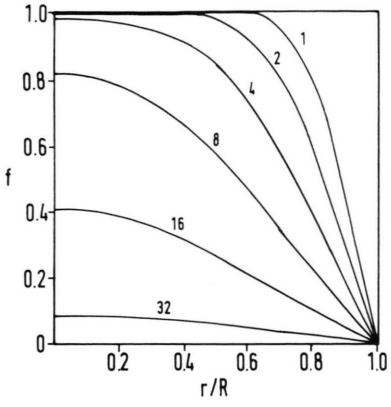

Fig. 7. Local variation of the penetration function $f(r, t)$ for different normalized times $t^* = 100\, t/T_{\mathrm{Diff}}$.

tion) p_{O_2} other than the time constants of the evolution of $1/T_1$. Here, oxidation results in a remarkably shorter time constant than reduction. As shown below, from the findings one can conclude that the conductivity part σ_2 is caused by majority charge carriers, while $1/T_1$ is induced by minority carriers, whose number is controlled by the actual concentration of the majority carriers.

The time response of σ is governed by the evolution of the local concentration $c(r, t)$ of the predominant carriers (O_i'', h$^\bullet$) in space and time according to Fick's second law, $\frac{\partial}{\partial t} c = D^c \nabla^2 c$, where D^c is the chemical diffusion coefficient.

The general solution of the equation can be written as [17]

$$c(r, t) = c_\infty + \beta\, c_0\, f(r, t) \tag{17}$$

where $\beta = (c_0 - c_\infty)/c_0 = 1 - \alpha$ denotes the relative difference between the equilibrium concentration before, (c_0) and after, (c_∞), the p_{O_2}-change. For a spherical sample with radius R the local variation of the penetration function $f(r, t)$ is plotted in Fig. 7 for different normalized times $t^* = 100\, t/T_{\mathrm{Diff}}$ with $T_{\mathrm{Diff}} = R^2/D^c$ being the characteristic diffusion time. Note that the time dependence of the function f does not depend on the magnitude and sign of β. The time evolution of the conductivity $\sigma(t)$ is given by the spatial average of (17):

$$\sigma(t) = \sigma_\infty + \beta \sigma_0 \int \mathrm{d}^3 r\, f(r, t). \tag{18}$$

As measured in the experiments (see Fig. 5), the time response of $\sigma(t)$ is antisymmetric with respect to the sign of β, whereas the time constant of the evolution does not depend on the sign of β. The solid lines in Fig. 5 are fits to the data by means of (17) and (18) using penetration functions $f(r, t)$ as depicted in Fig. 7, and a value of $(1 \pm 0.3) \cdot 10^{-5}$ cm^2/s for the chemical diffusion coefficient D^c.

The corresponding time evolution of the local concentration c_α of the minority carriers $V_O^{\bullet\bullet}$ responsible for the measured transient of $1/T_1(t)$ (Fig. 6) is controlled by the local concentration c of the majority carriers (O_i'', h$^\bullet$) according to the corresponding mass action law (14), i.e. $c_\alpha(r, t) \cdot c(r, t) = \mathrm{const}$. Hence, the strength of the time variation of c_α, $\dot{c}_\alpha$ decreases with rising concentration c of the dominant carriers according to $\dot{c}_\alpha = -\mathrm{const}/c^2 \cdot \dot{c}$.

Analogous to (17), a penetration function

$$f_\alpha \equiv \frac{\{V_O^{\bullet\bullet}\}_t - \{V_O^{\bullet\bullet}\}_\infty}{\{V_O^{\bullet\bullet}\}_0 - \{V_O^{\bullet\bullet}\}_\infty} \tag{19}$$

can be defined for the evolution of the local concentration $c_\alpha(r, t)$ of the minority carriers:

$$c_\alpha(r, t) = c_\infty + \beta\, c_0\, f_\alpha(r, t). \tag{20}$$

The function $f_\alpha(r, t)$ is related to the function $f(r, t)$ by

$$f_\alpha = \frac{1}{\alpha(1/f - 1) + 1}. \tag{21}$$

The local variation of f_α is a plotted in Fig. 8 a for an oxidation process ($\alpha > 1$) and in Fig. 8 b for the corresponding reduction process ($\alpha < 1$) for different normalized times t^*. In contrast to the time dependence of $f(r, t)$, reduction results in a remarkably larger time

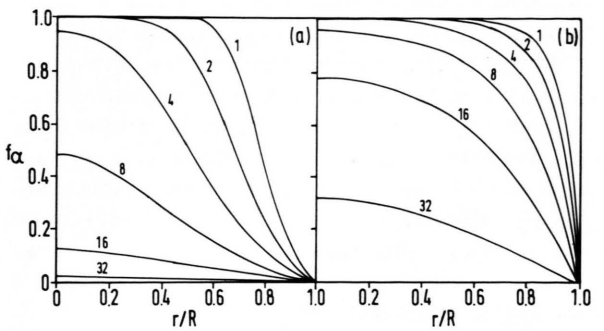

Fig. 8. Local variation of the penetration function f_α of the minority carriers at different normalized times $t^* = 100\, t/T_{\mathrm{Diff}}$. (a) oxidation ($\alpha = 5$); (b) reduction ($\alpha = 1/5$). Note the different response times of f_α for the two processes.

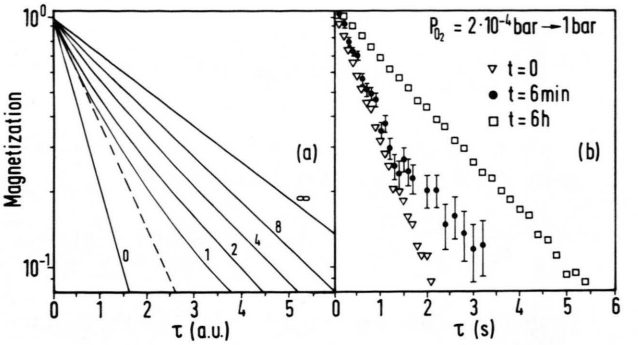

Fig. 9. Evolution of the nuclear magnetization $M(\tau)$ at different times after a sudden change of p_{O_2}. (a) Theoretical calculation, (22), for different normalized times $t^* = 100\, t/T_{\mathrm{Diff}}$ with $\alpha = 5$ (Dashed line: exponential), (b) Experimental data measured at 950 K.

constant of the penetration function f_α than oxidation, in agreement with the experimental findings shown in Figure 6. One should emphasize again that the difference in the time constants of the response of $1/T_1$ is a hint to the fact that the nuclear relaxation process is caused by minority carriers.

As the strength of the nuclear relaxation rate R is proportional to the concentration c_α i.e. $R(r,t) = R_0\, c_\alpha(r,t)$,an inhomogeneous spatial distribution of c_α leads to a non-exponential decay of the nuclear magnetization M. Supposing a steady-state concentration profile $c_\alpha(r, t = \mathrm{const})$ on the time scale of the T_1-experiment, the time evolution of $M = M(\tau)$ is given by

$$M(t;\tau) = \frac{1}{V_{\mathrm{ol}}} \int \mathrm{d}^3 r \exp(-R_0\, c_\alpha(r,t)\,\tau). \qquad (22)$$

Solutions of (22) are depicted in Fig. 9a for different normalized diffusion times t^* of the minority carriers. The calculations are in qualitative accord with the experimental observations presented in Figure 9b. The actual NSR rate $1/T_1$ was obtained from the initial slope of the magnetization decay, i.e. $1/T_1 = -\partial M(t,\tau)/\partial\tau|_{\tau=0}$.

The solid lines in Fig. 6 are fits to the NSR data by means of (19), (20), (21), and (22) using the same value of $(1 \pm 0.3) \cdot 10^{-5}$ cm^2/s for the chemical diffusion coefficient D^{c} as used for the fit procedure of $\sigma(t)$ (Figure 5).

As demonstrated by the experiments, the chemical diffusion coefficient is caused by the ambipolar diffusion of the majority carriers O_i'' and $h^\bullet$. The correspondent flux densities are coupled through the charge of the carriers by a Nernst field which reduces the drift motion of the rapid electronic defects ($h^\bullet$) and enhances the motion of the slowly moving oxygen interstitials (O_i''). Considering local electroneutrality ($j_{\mathrm{h}} = 2 j_{\mathrm{O_i}}$; $\{h^\bullet\} = 2\{O_i''\}$), the flux densities j_{h} and $j_{\mathrm{O_i}}$ of the two carriers can be written as [18]

$$j_{\mathrm{h}} = -D^{\mathrm{c}}\, \nabla\{h^\bullet\}, \quad j_{\mathrm{O_i}} = -D^{\mathrm{c}}\, \nabla\{O_i''\}. \qquad (23)$$

Here, the chemical diffusion coefficient D^{c} is related to the self-diffusion coefficients D_{h} and $D_{\mathrm{O_i}}$ of the holes and oxygen interstitials by

$$D^{\mathrm{c}} = \frac{3 D_{\mathrm{h}} D_{\mathrm{O_i''}}}{D_{\mathrm{h}} + 2 D_{\mathrm{O_i''}}} \sim 3 D_{\mathrm{O_i''}}. \qquad (24)$$

Because of $D_{\mathrm{h}} \gg D_{\mathrm{O_i}}$, the chemical diffusion is controlled by the slowly moving defects O_i''. The coupling due to the Nernst field is expressed by the factor 3 in (24).

7. Conclusions

Nuclear spin relaxation of ^{125}Te (NSR rate $1/T_1$) and electrical conductivity (σ) have been measured on α-TeO_2 as functions of both p_{O_2} and temperature. From the observed p_{O_2}-dependence of $1/T_1$ and σ a defect model is developed, which comprises the incorporation of oxygen at interstitial sites (O_i'') under formation of electron holes $h^\bullet$ and the formation of oxygen vacancies $V_O^{\bullet\bullet}$ by a Frenkel pair reaction. Comparison of the model of the experimental data reveals that the diffusion-induced part of $1/T_1$ is due to

the motion of $V_O^{\cdot\cdot}$, i.e.

$$\left.\frac{1}{T_1}\right|_{\text{Diff}} \propto \{V_O^{\cdot\cdot}\}/\Gamma_V \propto p_{O_2}^{-1/6} \exp\left(-\frac{H_F - \frac{1}{3}H_S - H_m}{kT}\right),$$

while the p_{O_2}-dependent contribution of the conductivity, σ_2, is caused by the diffusion of $h^{\cdot}$:

$$\sigma_2 \propto \mu_h \{h^{\cdot}\} \propto p_{O_2}^{-1/6} \exp\left(-\frac{\frac{1}{3}H_S}{kT}\right).$$

Evaluation of the data leads to 3.3 eV for the solution enthalpy H_S of oxygen and to 4.5 eV for the formation enthalpy H_F of oxygen Frenkel defects in α-TeO_2, using a value of 0.44 eV for the migration enthalpy H_m of the oxygen vacancies $V_O^{\cdot\cdot}$. Here, the mobility μ_h of the electron holes is supposed to be nearly temperature independent, whereas the motion of the vacancies $V_O^{\cdot\cdot}$ is given by thermally activated jumps with rate Γ_V.

Besides the p_{O_2}-dependent contribution to the conductivity, σ_2, two other contributions are observed. A high temperature contribution ($T \geq 900$ K), which is probably caused by intrinsic semiconduction, and a contribution which becomes significant below about 600 K; the latter is assumed to be related to the migration of impurity-controlled oxygen vacancies $V_O^{\cdot\cdot}$.

Measurements of the transients of $1/T_1$ and σ after a stepwise p_{O_2}-change suggest that the electron holes $h^{\cdot}$ and oxygen interstitials O_i'' are the predominant carriers with $2\{O_i''\} = \{h^{\cdot}\}$, whereas the oxygen vacancies $V_O^{\cdot\cdot}$ act as minority carriers. The chemical diffusion coefficient D^c is dominated by the diffusion of the slowly moving major defects O_i''; one obtains $D^c \approx 3D_{O_i}$ with D_{O_i} being the diffusion coefficient of the oxygen interstitials O_i''. Analysis of the transients of $1/T_1$ and σ leads to a uniform chemical diffusion coefficient D^c. At 950 K we obtained $D^c = (1 \pm 0.3) \cdot 10^{-5}$ cm^2/s.

Acknowledgements

The authors would like to thank Prof. H. Schmalzried for helpful discussions and Prof. H. Mehrer and M. Baumann for performing the ^{127}Te radio-tracer experiments. The work was financially supported by the Deutsche Forschungsgemeinschaft.

[1] T. Takizawa, J. Phys. Soc. Japan **48,** 505 (1980).
[2] G. Arlt and H. Schweppe, Sol. State Com. **6,** 783 (1968).
[3] N. Uchida and Y. Ohmachi, J. Appl. Phys. **40,** 4692 (1969).
[4] P. S. Peercy, I. J. Fritz, and G. A. Samara, J. Phys. Chem. Solids **36,** 1105 (1975).
[5] J. Wegener, R. Küchler, O. Kanert, and A. Watterich, Proceed. ICDIM92 (O. Kanert and J. M. Spaeth, eds.), World Scientific, Vol. 2, 715 (1993).
[6] G. K. White, S. J. Collocott, and J. H. Collins, J. Phys. Cond. Matt. **37,** 7715 (1990).
[7] H. Jain and A. S. Nowick, Phys. stat. sol. (a) **67,** 701 (1981).
[8] E. Hartmann and L. Kovács, Phys. stat. sol. (a) **74,** 59 (1982).
[9] J. Wegener, PhD thesis, Dortmund (1994).
[10] H. Kolem, O. Kanert, H. Schulz, and B. Günther, J. Magn. Res. **87,** 160 (1990).
[11] M. Durand, B. A. Yrault, Y. Marqueton, and E. A. Decamps, Phys. stat. sol. (b) **78,** 767 (1976).
[12] A. Abragam and B. Bleaney: Electron Paramagnetic Resonance of Transition Ions, Clarendon, Oxford 1970, p. 547 ff.
[13] N. Bloembergen and T. J. Rowland, Phys. Rev. **97,** 1679 (1955).
[14] Y. S. Hwang and R. E. Norberg, Phys. Rev. **B 14,** 3765 (1976).
[15] D. W. Davies, The theory of the electric and magnetic properties of molecules, John Wiley & Sons, New York 1967.
[16] O. Kanert, Physics Report **91,** 185 (1982).
[17] J. Crank, The Mathematics of Diffusion, Clarendon Press, Oxford 1955, p. 69 ff.
[18] J. Philibert: Atom movements, Diffusion and Mass Transport in Solids. Les Editiones de Physique, Les Ulis, France 1991, p. 224 ff.